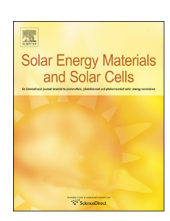
FISEVIER

Contents lists available at ScienceDirect

Solar Energy Materials and Solar Cells

journal homepage: www.elsevier.com/locate/solmat



Titanium nitride nanoparticles for the efficient photocatalysis of bicarbonate into formate



Alyssa Beierle^{a,1}, Paul Gieri^{c,1}, Hanqing Pan^b, Michael D. Heagy^b, Alejandro Manjavacas^{c,*}, Sanchari Chowdhury^{a,**}

- ^a Department of Chemical Engineering, New Mexico Institute of Mining and Technology, Socorro, NM, 87801, United States
- Department of Chemistry, New Mexico Institute of Mining and Technology, Socorro, NM, 87801, United States
- ^c Department of Physics and Astronomy, University of New Mexico, Albuquerque, NM, 87131, United States

ARTICLE INFO

Keywords: Plasmon Photocatalysis Titanium nitride Titanium dioxide Bicarbonate Formate

ABSTRACT

Metallic nanoparticles can act as efficient photocatalysts thanks to the surface plasmons that they support, which are capable of harvesting light and generating hot carriers. Recently, titanium nitride (TiN) nanostructures have emerged as promising candidates for this application due to their much lower cost, and therefore greater sustainability, than structures made of noble metals, as well as their expected long-term thermal stability. In this work, we demonstrate that, under solar illumination, TiN nanoparticles, in combination with titanium dioxide (TiO₂) nanostructures, can significantly increase the photocatalytic production of formate through the simultaneous photoreduction of bicarbonate and oxidation of glycerol. Importantly, we also show that TiN nanoparticles alone can provide an enhancement of the photocatalytic efficiently when compared to TiO_2 nanocatalysts. Furthermore, by characterizing the morphology and material properties of the TiN nanoparticles after the reaction, we confirm that they remain stable under reaction conditions for extended periods of solar light exposure (8 hours). The results of this work advance our understanding of TiN nanoparticles as efficient photocatalysts and their use for the production of valuable chemicals.

1. Introduction

Metallic nanostructures have gained a great deal of attention for their potential as efficient photocatalysts [1-7]. These nanostructures support strong charge oscillations, commonly referred to as plasmons, when illuminated with light in the visible and near infrared part of the spectrum. Surface plasmons interact strongly with light and confine it into small volumes, thus leading to a significant enhancement of the electromagnetic field in their vicinity [8]. After excitation, plasmons decay following two possible paths: (i) radiating their energy away from the nanostructure in the form of scattered photons, and (ii) generating a nonthermal population of electrons and holes [6,9,10]. These hot carriers can then thermalize, releasing their energy to the nanoparticle and its surroundings as heat [11,12], or they can be transferred to neighboring systems, such as adsorbed reactant molecules or nanostructures [5,13,14]. Since the energy of the plasmon-induced hot carriers is usually well above the Fermi level of the nanostructure, these excitations can drive chemical reactions, which would otherwise require a large energy supply [6]. This effect has already been demonstrated for a large variety of chemical reactions, including water splitting [15–22], hydrogen and oxygen dissociation [23–25], and the generation of hydrogen from ethanol [26], to name a few. Additionally, the hot carriers can be transferred to the conduction band of neighboring semiconductor photocatalysts, such as titanium dioxide (TiO₂) [27]. This has a twofold purpose: on one hand it helps to increase the carrier lifetime, thus facilitating its transfer to reactant molecules [5,28], and, on the other hand, it improves the photocatalytic performance of the semiconductor by allowing the use of photons with energies below its bandgap [29,30].

The majority of the research efforts on plasmonic photocatalysis have been focused on the use of noble metals such as gold and silver [5,6,31–34]. These traditional plasmonic materials are chosen because they support strong plasmonic resonances in the visible range of the spectrum [35]. However, due to their scarcity, and consequently high cost, the use of these materials lacks the sustainability required for large-scale industrial applications. Furthermore, these materials usually

^{*} Corresponding author.

^{**} Corresponding author.

 $[\]textit{E-mail addresses:} \ manjavacas@unm.edu \ (A.\ Manjavacas), \ sanchari.chowdhury@nmt.edu \ (S.\ Chowdhury).$

¹ Authors contributed equally to this paper.

show poor long-term stability in the type of environments found in many industrial settings [36]. This is particularly true in oxidative (for silver) or high temperature (for gold and silver) environments, where the particles are likely to reshape, leading to a change in the plasmon resonance frequency, or to oxidize away entirely.

These limitations have prompted a global search for alternative plasmonic materials. Recent works have shown, for instance, that aluminum nanoparticles under laser illumination can be used to dissociate hydrogen [37]. Other interesting candidates that have been proposed are metal nitrides such as TiN and ZrN [38-47]. In particular, TiN nanostructures have been shown to support strong surface plasmons, with broad resonances overlapping most of the visible spectrum [39,48]. Furthermore, for the same dimensions, TiN nanostructures show larger integrated absorption cross sections than gold or silver particles, allowing for significantly higher solar photocatalytic efficiencies [38,49,50]. TiN also has its Fermi energy aligned with that of the commonly used photocatalytic semiconductor TiO₂ [42]. Therefore, unlike gold and silver, which form Schottky interfaces with TiO2, TiN forms an Ohmic interface, thus facilitating the transfer of hot electrons [45,51]. In addition to its plasmonic properties, TiN also has a much higher melting temperature than silver and gold, which results in a better long-term stability, and enables its use in applications requiring high temperature environments [52-55]. TiN is also significantly cheaper than gold and silver, which makes it more sustainable than traditional plasmonic materials [39,40]. For all of these reasons, TiN nanostructures are being investigated with the objective of using them to enhance a number of photocatalytic reactions [45,46,56-60].

One reaction of particular interest that can benefit from this enhancement is the production of formic acid [61]. This chemical is in high demand for its use in hydrogen storage [62] and as a preservative in a significant number of industries [61]. In addition to this, formic acid is a commonly used intermediate species for the synthesis of many valuable chemicals, such as methanol [61,63]. Unfortunately, the high reduction potential required in the production of these chemicals makes necessary the use of semiconductor photocatalysts with large bandgap, such as TiO2, ZnO, and ZnS [64,65]. However, these materials are only capable of absorbing photons in the UV/near-UV range, which hinders the possibility of efficiently utilizing solar light to drive these reactions, since much of the solar spectrum lies below the bandgap [39,41]. Previous work has shown that, by incorporating traditional plasmonic materials, such as gold, into the TiO2 photocatalyst, a significant enhancement of the reduction rate of bicarbonate to formate, the anion derived from formic acid, can be achieved [33]. However, as discussed previously, due to the limitations of those materials, it is important to explore alternative plasmonic photocatalysts, such as TiN, that could enhance this reaction.

In this study, we investigate the use of TiN nanostructures for the enhancement of the photocatalytic reduction of bicarbonate into formate. We show that the formate production rate achieved using ${\rm TiO_2}$ nanostructures, under solar light, is enhanced by six times with the addition of TiN nanoparticles. Importantly, we find that even TiN nanoparticles alone, *i.e.*, without the ${\rm TiO_2}$ nanostructures, also achieve a significant enhancement of the production rate. Additionally, we investigate the chemical stability of TiN for this experiment, showing that the nanoparticles do not show appreciable degradation during the reaction. Our results shed light into the use of TiN nanoparticles for plasmon-enhanced photocatalysis.

2. Materials and Methods

2.1. Photocatalysts

The TiO_2 photocatalyst was purchased from Sigma-Aldrich (Aeroxide $^{\circ}$ P25). According to the manufacturer's data, the TiO_2 nanoparticles have a specific surface area of 35–65 m 2 /g (BET) and a mean diameter of 21 nm. TiN nanoparticles were purchased from US

Research Nanomaterials, Inc. The morphology and material properties of all of the nanoparticles were characterized using transmission electron microscopy (TEM), high-resolution TEM (HRTEM), and energy-dispersive X-ray spectroscopy (EDX), all performed using a JEOL-2010 transmission electron microscope. Furthermore, we also employed UV–Vis spectroscopy on a Thermo Scientific Evolution 260 Bio UV–Vis spectrophotometer with integrating sphere, X-ray powder diffraction (XRD) on a X'Pert Pro XRD instrument, and Raman spectroscopy on a HORIBA Jobin-Yvon LabRAM Aramis micro-Raman system (see the Supporting Information).

2.2. Photocatalytic reactions

The starting reactant for the bicarbonate to formate reaction consisted of a buffer made of $0.3\,\mathrm{M}$ NaHCO $_3$, with $2\,\mathrm{M}$ hole scavenger glycerol, and Milli-Q water. The photocatalytic reaction occurred on a Petri dish. We studied three different photocatalysts, namely P25 TiO $_2$ nanoparticles, 20 nm TiN nanoparticles, and an even mixture of the two. All of them were spin coated onto the Petri dishes, using a catalyst solution with a concentration of $10\,\mathrm{mg/mL}$, and characterized using scanning electron microscopy (SEM) in a Hitachi S-4100 scanning electron microscope.

Using this setup, we performed two types of catalytic experiments. In the first case, the reactions were conducted under solar simulated light, using an ABET Technologies SunLite™ with AM 1.5 (or AM 0) filter and a 1000 W xenon arc lamp producing 1000 W/m², and kept at isothermal conditions at room temperature (22°C) using a fan. In the second case, the experiment was conducted in the dark under isothermal conditions at 40°C using a hot plate. In all cases, aliquots were collected every 2 hours, and we used ion chromatography to quantify the concentration of formate. The ion chromatography (IC) was performed using a Dionex AS50 IC with a Dionex IonPac ICE-AS6 ion exclusion column, and a Thermo Scientific Dionex AMMS-ICE 300 suppressor. The IC instrument was equipped with a Dionex CD25 conductivity detector. The reagents used were 0.4 mM heptafluorobutyric acid as the eluent, at a flow rate of 1.2 mL/min, and 5 mM tetrabutylammonium hydroxide as the regenerate. The reaction products on the photocatalysts were also characterized using Fouriertransform infrared spectroscopy (FTIR) performed in a Thermo Scientific Nicolet IS50 FTIR spectrometer with integrating sphere.

In order to analyze the stability of the TiN photocatalysts, we recovered them from the reactor after 8 hours of reaction, washed them to eliminate the other reaction components, and characterized their morphology and material properties using HRTEM and XRD. The results were compared with similar analysis of pristine TiN photocatalysts.

2.3. Theoretical modeling

The absorption cross sections of the different photocatalysts were calculated by solving Maxwell's equations using Mie theory [66] for spherical multishell structures, and a commercially available Finite Element Method (FEM) Solver, COMSOL Multiphysics, for elliptical multishell nanoparticles. In all cases, we performed an average over all possible incidence directions and polarizations. The dielectric functions of TiN and TiO_2 were modeled using tabulated data from Refs. [38,67], respectively, while for Au and Ag we used data from Ref. [68].

For the absorbed power calculations, we used the AM 1.5 Global tilt solar intensity spectrum [69], which was multiplied with the absorption cross sections to obtain the absorbed power per wavelength. The total absorbed power was calculated by integrating these results.

3. Results and discussion

The photocatalytic process under investigation is depicted in Fig. 1 (a). Simulated solar light is used to excite surface plasmons in the TiN

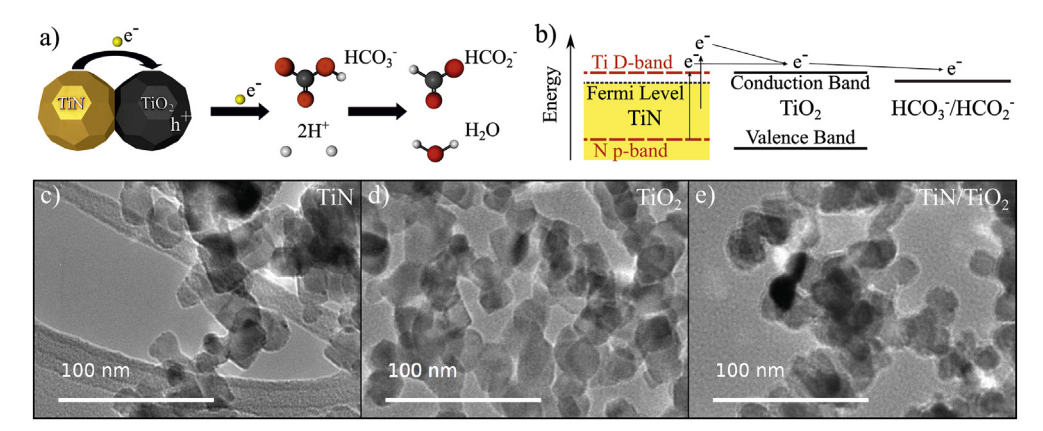


Fig. 1. (a) Schematic for the photocatalytic reduction of bicarbonate (HCO_3^-) into formate (HCO_2^-). (b) Energy level diagrams for hot electron transfer in the reaction of interest. (c)–(e) TEM images of the TiN, TiO₂, and TiN/TiO₂ composite photocatalysts.

nanoparticles, which, upon decaying, produce hot carriers that are transferred to the conduction band of the ${\rm TiO_2}$ nanoparticles. This transfer is facilitated by the Ohmic interface formed between TiN and TiO₂, which is illustrated in Fig. 1(b), and has been experimentally characterized in previous works [45] (see also Fig. S5 and the corresponding discussion in the Supporting Information). This Ohmic interface also enables the use of the carriers generated through direct photon absorption from interband transitions in TiN [41,45], as well as those generated from transitions between the valence and conduction bands of ${\rm TiO_2}$ by photons in the UV part of solar spectrum that have energies above the ${\rm TiO_2}$ band gap.

The hot carriers in the conduction band of TiO2 are then injected into the reactants to accomplish the reduction of bicarbonate to formate. This is aided by the approximate alignment of the conduction band of TiO_2 with the reduction energy level of bicarbonate [70–72], as well as by the presence of glycerol, which acts as an efficient hole scavenger and produces the protons required for the bicarbonate reduction. The use of a hole scavenger is crucial to ensure the nanoparticles remain electrically neutral, thus allowing for a continuous flow of electrons from the photocatalyst to the bicarbonate. The efficiency of glycerol as a hole scavenger for the photoreduction of bicarbonate to formic acid on TiO2, which has been demonstrated in the past [64], is related to the fact that it contains one secondary and two primary alcohol groups, all of which constitute potential sites for oxidation that enhance their hole scavenging activity. This is consistent with density functional theory-based theoretical calculations that have also established glycerol as a more efficient hole scavenger for TiO2 than other organic solvents like tert-butanol, 2-propanol, methanol, and formic acid [73]. It is worth noting that efficient hole scavenging from both ${\rm TiO_2}$ and ${\rm TiN}$ is also important for preventing charge recombina-

The primary reactions of the photochemical process under study are as follows [72]:

$$TiO_2(2e^-) + HCO_3^- + 2H^+ \rightarrow TiO_2 + HCO_2^- + H_2O,$$
 (1)

$$TiO_2(h^+) + C_3H_8O_3 \rightarrow TiO_2 + Oxidized products + H^+,$$
 (2)

while two important secondary reactions are:

$$TiO_2(h^+) + H_2 O \rightarrow TiO_2 + H^+ + {}^{\bullet}OH,$$
 (3)

$$HCO_3^- + {}^{\bullet}O H \rightarrow {}^{\bullet}CO_3^- + H_2O.$$
 (4)

In reaction (1), the bicarbonate (HCO_3^-) is reduced to formate (HCO_2^-) and water by the electrons in the conduction band of TiO_2 . At the same time, in reaction (2), glycerol ($C_3H_8O_3$) scavenges the holes from the valence band of TiO_2 to produce different oxidized products and the protons necessary for reaction (1). Upon oxidation, glycerol is likely first dehydrogenated to glyceraldehyde and 1,3-

dihydroxyacetone, which, subsequently, can be further oxidized by hot holes with water to produce hydroacetic and formic acid through C–C bond cleavage [74,75]. It is important to note that the contribution of formate arising from glycerol oxidation is usually negligible in comparison to the bicarbonate reduction reaction [33]. Happening in parallel to the primary reactions, there are two important secondary reactions. In (3), water reacts with any hot holes left in the photocatalyst, producing protons and hydroxyl radicals. The latter can lead to reaction (4), in which bicarbonate reacts with hydroxyl radicals, and therefore competes with the primary reaction (1). In the absence of hole scavengers, the amount of hydroxyl radicals from the photooxidation of water is directly proportional to the concentration of bicarbonate in solution [72]. However, thanks to the use of glycerol, which eliminates the holes and hydroxyl radicals, we can limit this competing reaction, thus improving the production of formate.

In order to investigate the enhancement of the photocatalytic production of formate provided by TiN nanoparticles, we perform experiments for three different nanocatalysts: (i) TiO2 nanoparticles, (ii) TiN nanoparticles, and (iii) an even mixture of TiN/TiO2 nanoparticles. TEM images of each of these composites are shown in Fig. 1(c)-(e), respectively. The TiO2 and TiN nanoparticles have average diameters of 21 and 20 nm, respectively, with the TiN structures displaying a 1-2 nm amorphous TiO₂ shell (see Fig. 5). The TiO₂ particles are made mostly of anatase phase (80%) with the rest being rutile phase (20%) (see the Supporting Information). As explained in the Materials and Methods section, for the photocatalysis experiments, the TiO2 and TiN nanoparticles are deposited onto a glass Petri dish by spin coating a catalyst solution of concentration of 10 mg/mL. After deposition, the particles tend to aggregate and form conglomerates with sizes between 50 and a few hundreds nanometers, as can be seen in the TEM images shown in Fig. 1(c)-(e).

The photocatalytic reaction is driven by the absorption of solar light, which is dominated by the TiN nanoparticles because TiO2 only absorbs photons with energies above its bandgap (\approx 3.2 eV). Therefore, it is important to analyze the absorption characteristics of the TiN nanostructures. To that end, we measure the absorbance of these nanostructures in solution using UV-Vis spectroscopy, and compare those results to theoretical calculations shown in Fig. 2(a). The black dashed curve represents the experimentally measured absorbance, while the black solid curve corresponds to the calculations for a spherical TiN nanoparticle with a total diameter of 20 nm, including a 2 nm TiO₂ shell. The results of these calculations are in reasonable agreement with the experimental measurements. In particular, both spectra display an absorption band centered around 750 nm that extends over a significant portion of the visible spectrum, thus making these structures ideal for harvesting solar light. As expected, the nanoparticle also display a strong absorption below 450 nm, which is associated with interband

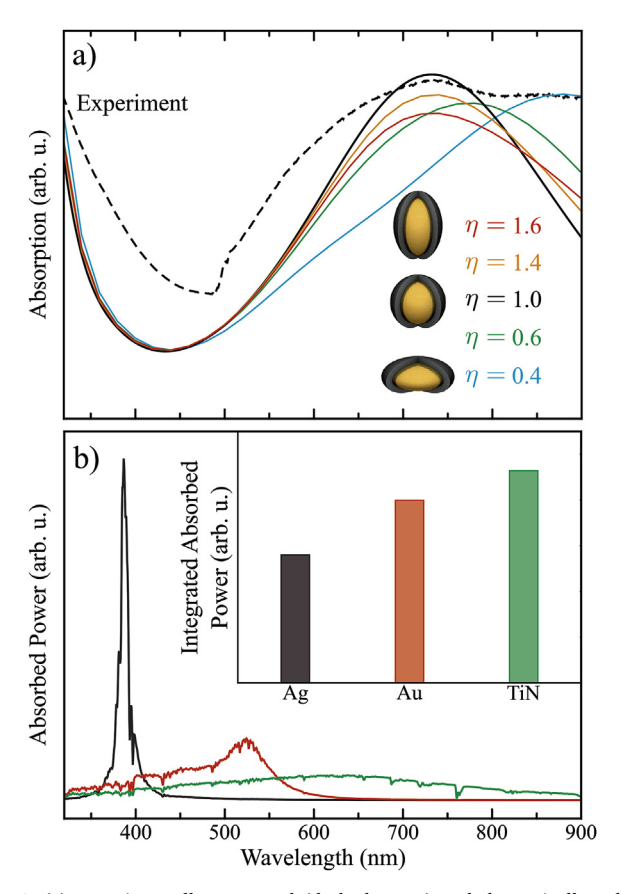


Fig. 2. (a) Experimentally measured (dashed curve) and theoretically calculated absorption spectra for different TiN nanoparticles in water (solid curves). The black curve stands for the results obtained for a spherical TiN nanoparticle with 20 nm diameter, including a 2 nm TiO₂ shell. To account for the dispersion of sizes and shapes in the experiment, we model four different ellipsoidal coreshell nanostructures, as indicated in the legend. All of these structures have the same core volume of TiN as the spherical particle with a 2 nm TiO2 shell, and their geometry is characterized by the parameter η , which represents the ratio between the diameters along the vertical and horizontal axes. (b) Absorbed power spectrum calculated for spherical nanoparticles with 20 nm diameter made of silver (black curve), gold (red curve), and TiN (green curve), placed in water, when illuminated with the AM 1.5 solar spectrum (see Materials and Methods section). The inset shows the integrated power absorbed for each nanoparticle over the wavelength range from 320 to 900 nm. (For interpretation of the references to colour in this figure legend, the reader is referred to the Web version of this article.)

transitions.

That said, we observe that the experimental spectrum has a much broader absorption band than the theoretical calculations, and, at large wavelengths, it displays a second absorption peak. We attribute these differences to the dispersion in the morphology of the nanoparticles measured in the experiment [76,77]. To confirm our hypothesis, we perform calculations for four different ellipsoidal core-shell nanostructures, all of them with the same core volume of TiN as the spherical nanoparticle analyzed above and a 2 nm TiO2 shell. The geometry of these nanostructures is characterized by the parameter η , which represents the ratio between the vertical and the horizontal diameters. Therefore systems with $\eta > 1$ are prolate ellipsoids, while those with $\eta < 1$ are oblate. Examining these results, we observe that for the prolate particles (yellow and red curves), the absorption band decreases in strength and becomes broader. On the other hand, for the oblate particles (green and blue curves), there is an overall redshift, which for $\eta = 0.4$ results in a resonance that lines up with the secondary peak seen in the experimental absorbance. This analysis shows that changes in the particle morphology lead to modifications in the absorption spectra that

can explain the differences found between the experimental and the theoretical results.

It is very illustrative to compare the absorption performance of the TiN nanoparticles with that of similar nanostructures made of conventional plasmonic materials, such as gold and silver. To that end, in Fig. 2(b), we plot the absorbed power spectrum for spherical nanoparticles with 20 nm diameter made of silver (black curve), gold (red curve), and TiN (green curve), placed in water, when illuminated with the standard AM 1.5 solar spectrum (see the Materials and Methods section). In this case, to ensure a fair comparison, we do not consider a TiO₂ shell on the TiN nanoparticles. Examining these results, we observe that the absorption peak, associated with the plasmon resonance. of gold, and especially silver, nanoparticles is significantly stronger than that of the TiN nanoparticle. However, these resonances are much narrower and therefore they may lead to a smaller integrated absorption. This is confirmed in the inset, where we plot the absorbed power integrated over the wavelength range from 320 to 900 nm. Despite having significantly smaller peak absorption than either silver or gold, the broad response of TiN leads to a larger overall absorption efficiency, which is crucial for any application utilizing solar light.

In order to analyze the production of formate for each of the three photocatalysts under investigation (TiO2, TiN, and TiN/TiO2 composites), we submerse the reactors loaded with the photocatalysts in a buffer solution containing 3 M glycerol and 0.2 M bicarbonate prepared with ultrapure water. The particle concentration on the reactor is approximately 200 particles/ μ m². The photocatalytic reaction is run for a period of 8 hours under isothermal conditions at 22°C. For the light source, we use an AM 1.5 solar simulator. The concentration of formate in solution is measured using ion chromatography. The corresponding results throughout the 8 hours of reaction time are shown in Fig. 3(a) for the three photocatalyst under investigation. Clearly, the largest formate production is obtained for the TiN/TiO₂ composite, while the minimum corresponds to the TiO₂ nanoparticles alone. The formate production rate is plotted in panel (b). We find that TiO₂ nanoparticles alone have a productivity of approximate 1035 mmol/hr per gram of photocatalyst, while for the TiN/TiO2 nanocomposite we obtain approximate 3080 mmol/hr/g. These values correspond to an absolute productivity of 0.834×10^{-2} mmol/hr and 2.609×10^{-2} mmol/hr, respectively. However, we need to remark that for the TiN/TiO2 composite, the total particle loading is the same as for the TiO2 nanoparticles alone, meaning that the amount of TiN and TiO2 in the composite photocatalyst is exactly half. Therefore, we conclude that the addition of TiN nanoparticles enhances the formate production rate of TiO_2 nanoparticles alone by a factor of ≈ 6 . Importantly, TiN nanoparticles alone also enhance the formate production, resulting in a rate ≈2 times higher than that of TiO₂ nanoparticles alone. This could be facilitated by the 1-2 nm thick layer of TiO2 present on the surface of the TiN nanoparticles [78]. It should be noted as well that the productivity of TiN/TiO2 composite is more than the simple average of the productivity of TiN and TiO2.

To complete the characterization of the performance of the different photocatalysts, we measure the formate production for TiN/TiO_2 composites with different mix ratios of TiN to TiO_2 . Analyzing the corresponding results, which are shown in Fig. S6 of the Supporting Information, we find that mix ratio has an impact on the production of formate, with the 1:1 mix resulting in the largest formate production.

The experimental results confirm that the TiN nanoparticles enhance the efficiency of the photocatalytic production of formate. However, it is crucial to determine if this enhancement is produced by the hot carriers provided by the TiN nanoparticles, or if it is caused just by an increase of their temperature. As previously discussed, TiN nanoparticles exhibit a large absorption under solar light, and, despite the solution being kept under isothermal conditions, it is possible that the nanoparticles are at a higher temperature than the solution. Indeed, previous works have shown that thermal energy from optically excited plasmons can be used to drive reactions [6,43,45]. In our particular

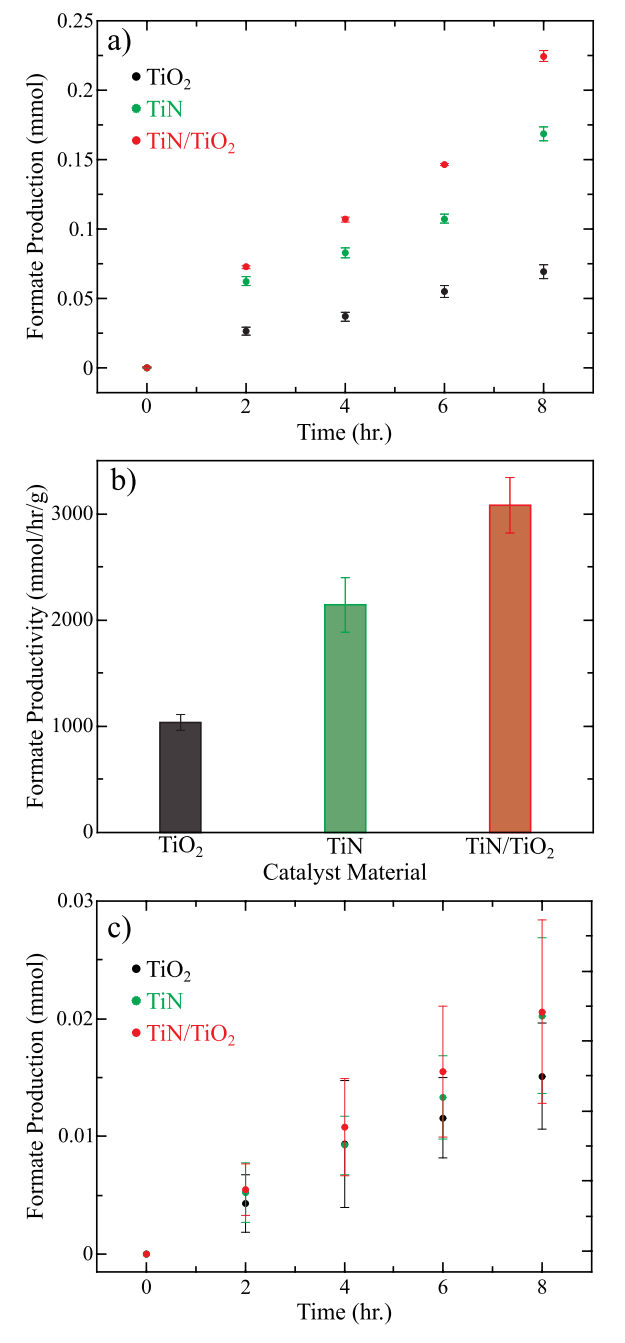


Fig. 3. (a) Formate production measured as a function of time for the TiO_2 , TiN, and TiN/TiO_2 composite photocatalysts, under simulated solar light at constant $22^{\circ}C$ temperature. (b) Formate productivity per hour for each photocatalyst. (c) Formate production as a function of time in the dark at $40^{\circ}C$.

case, we estimate the temperature of the nanoparticle following the approach of [11], from the balance between the integrated power that it absorbs, which is calculated in Fig. 2(b), and the energy transfer to water through contact. We obtain a negligible temperature increase, mainly because the relatively small power of the solar illumination ($\approx 1 \, \text{kW/m}^2$), as well as the large thermal conductivity of water.

To confirm that thermal effects do not cause the enhancement of the reaction, we perform a control experiment in the dark with the solution kept at a temperature of 40° C. The results of this experiment, which is done for all three photocatalysts, are shown in Fig. 3(c). We find that, under these conditions, the production of formate when TiN nanoparticles are present is an order of magnitude smaller than under solar irradiance.

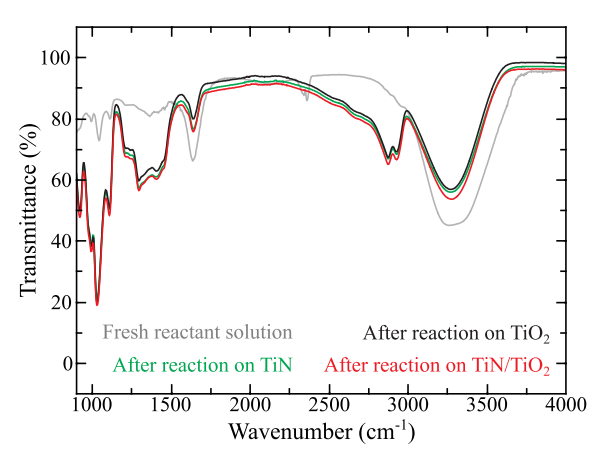


Fig. 4. Comparison of the FTIR spectrum of the fresh reactant solution (gray curve), with the corresponding spectra of the reaction products adsorbed on the ${\rm TiO_2}$ (black curve), TiN (green curve), and ${\rm TiN/TiO_2}$ composite (red curve) photocatalysts, measured after 8 hours of isothermal photocatalytic reaction at 22°C. (For interpretation of the references to colour in this figure legend, the reader is referred to the Web version of this article.)

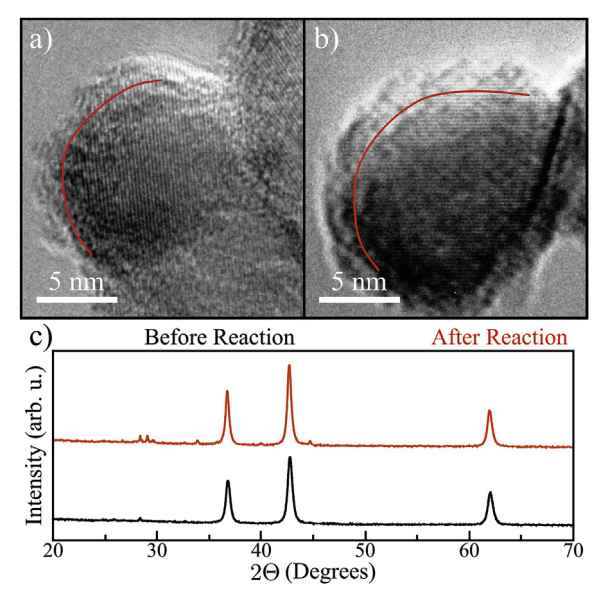


Fig. 5. (a,b) HRTEM images of a TiN photocatalyst before (a) and after (b) 8 hours of isothermal photocatalytic reaction at 22° C, under simulated solar light. In both cases, the red curve indicates the approximate interface between the TiN core and the TiO₂ shell. (c) X-ray diffractogram of a TiN photocatalyst before and after reaction. (For interpretation of the references to colour in this figure legend, the reader is referred to the Web version of this article.)

In order to obtain a complete picture of the photocatalytic reaction occurring on the different photocatalysts under investigation, we perform Fourier transform infrared spectroscopy (FTIR) before and after the reaction. The gray curve of Fig. 4 shows the results measured before reaction for the fresh reactant solution, while the other curves correspond to the FTIR spectra of the reactants adsorbed on the TiO₂ (black curve), TiN (green curve), and TiN/TiO₂ composite (red curve) photocatalysts, measured after 8 hours of isothermal photocatalytic reaction at 22° C, under solar illumination. Examining the FTIR spectra, we observe a broad peak at 3250 cm⁻¹, which arises from the alcohol groups of glycerol [79]. This peak is present for the fresh reactant solution, as well as for all of the different photocatalysts after reaction. However, as expected, its intensity decreases after the reaction, due to the oxidation of glycerol. This is further supported by the appearance, after the reaction, of a peak at 2830 cm⁻¹, corresponding to aldehyde, probably

due to the formation of glyceraldehyde, which is an oxidation product of glycerol [79]. Similarly, the peak at 1050 cm⁻¹ is characteristic of alcohol and is likely due to the formation of 1,3-propanediol, another oxidation product of glycerol [79]. On the other hand, the peaks appearing between 1290 and 1400 cm⁻¹ can be attributed to the CO and COO stretching modes, respectively [80]. These peaks, which increase after the reaction, are indicative of the presence of formic acid and formate [80]. Therefore, the FTIR data confirms the reduction of bicarbonate to formate. Furthermore, it also corroborates the oxidation of glycerol, thus supporting its role as hole scavenger, even for the TiN photocatalyst, and highlighting its importance for the efficient extraction of hot electrons from these plasmonic nanostructures.

Any large-scale use of the enhancement of the photocatalytic production of formate provided by TiN nanoparticles would require these nanostructures to remain stable after the reaction. In principle, it is well known that TiN has a high melting temperature, well above that of gold and silver. However, it is also important to confirm that the nanoparticles remain oxidatively stable during the reaction, since any increase in the native oxide layer thickness would lead to a decrease in the size of the TiN core, and therefore to a redshift in the plasmon resonance as well as a decrease in the overall absorption. To check the stability of the TiN photocatalysts, we recovered them from the reactor after 8 hours of isothermal photocatalytic reaction at 22°C, under solar light, and washed them to get rid of the reaction components. Then, we examined the morphology of the oxide layer on the surface of the TiN nanoparticles using HRTEM images of the nanoparticles taken before and after the reaction, which are shown in Fig. 5(a) and (b), respectively. These images confirm that the oxide layer remains of the same thickness. Furthermore, we compared the X-ray diffractogram of the nanoparticles before and after being used. As can be seen from the corresponding results plotted in Fig. 5(c), the TiN mostly shows the rock-salt crystal structure of osbornite, thus confirming that its structure remains stable under reaction conditions. It is worth noting, as well, that we do not observe any decrease in the photocatalytic performance of the nanostructures over the course of the reaction in any of the experiments performed, which further supports the stability of the TiN nanostructures.

4. Conclusions

In summary, we have shown that TiN nanoparticles can serve as an efficient photocatalyst for the reduction of bicarbonate into formate under solar illumination. The main reasons behind this enhancement are (i) the broad plasmonic resonances that TiN nanoparticles support, which allows for an efficient utilization of the whole solar spectrum, and (ii) the Ohmic interface they form with the commonly used photocatalyst TiO_2 , which allows for an efficient transfer of the plasmoninduced hot carriers to the reactants. Indeed, our results suggest that TiN could be also used to improve the performance of other semiconductor photocatalysts such as ZnO, CdS, or Fe_2O_3 . In addition, we have shown that the TiN nanoparticles remain stable during the photocatalytic reaction. The results of this work improve our understanding of the photocatalytic properties of TiN nanoparticles arising from their plasmonic response, and therefore serve to pave the way to develop efficient and sustainable photocatalysts for real-world applications.

Acknowledgements

This work has been partially sponsored by the US National Science Foundation (Awards IIA-1301346 and ECCS-1710697), and has been performed, in part, at the Center for Integrated Nanotechnologies, an Office of Science User Facility operated for the U.S. Department of Energy Office of Science by Los Alamos National Laboratory (Contract DE-AC52-06NA25396) and Sandia National Laboratories (Contract DE-NA-0003525). The authors want to thank Dustin Baca for IC assistance and Ying-Bing Jiang for TEM assistance, and acknowledge the UNM

Center for Advanced Research Computing for the computational resources used in the theoretical modeling. PG thanks financial support from the UNM NSMS program through the Whitten Family Fellowship and the Graduate Assistance in Areas of National Need (GAANN) fellowship.

Appendix A. Supplementary data

Supplementary data to this article can be found online at https://doi.org/10.1016/j.solmat.2019.109967.

References

- S. Linic, P. Christopher, D.B. Ingram, Plasmonic-metal nanostructures for efficient conversion of solar to chemical energy, Nat. Mater. 10 (2011) 911–921.
- [2] P. Christopher, H. Xin, S. Linic, Visible-light-enhanced catalytic oxidation reactions on plasmonic silver nanostructures, Nat. Chem. 3 (2011) 467–472.
- [3] A. Marimuthu, J. Zhang, S. Linic, Tuning selectivity in propylene epoxidation by plasmon mediated photo-switching of cu oxidation state, Science 339 (2013) 1590–1593.
- [4] W. Hou, S.B. Cronin, A review of surface plasmon resonance-enhanced photocatalysis, Adv. Funct. Mater. 23 (13) (2013) 1612–1619.
- [5] C. Clavero, Plasmon-induced hot-electron generation at nanoparticle/metal-oxide interfaces for photovoltaic and photocatalytic devices, Nat. Photon. 8 (2014) 95–103.
- [6] M.L. Brongersma, N.J. Halas, P. Nordlander, Plasmon-induced hot carrier science and technology, Nat. Nanotechnol. 10 (2015) 25–34.
- [7] L. Zhou, D.F. Swearer, C. Zhang, H. Robatjazi, H. Zhao, L. Henderson, L. Dong, P. Christopher, E.A. Carter, P. Nordlander, N.J. Halas, Quantifying hot carrier and thermal contributions in plasmonic photocatalysis, Science 362 (2018) 69–72.
- [8] J.A. Schuller, E.S. Barnard, W. Cai, Y.C. Jun, J.S. White, M.L. Brongersma, Plasmonics for extreme light concentration and manipulation, Nat. Mater. 9 (3) (2010) 193–204.
- [9] A.O. Govorov, H. Zhang, Y.K. Gun'ko, Theory of photoinjection of hot plasmonic carriers from metal nanostructures into semiconductors and surface molecules, J. Phys. Chem. C 117 (32) (2013) 16616–16631.
- [10] A. Manjavacas, J.G. Liu, V. Kulkarni, P. Nordlander, Plasmon-induced hot carriers in metallic nanoparticles, ACS Nano 8 (2014) 7630–7638.
- [11] G. Baffou, R. Quidant, F.J. García de Abajo, Nanoscale control of optical heating in complex plasmonic systems, ACS Nano 4 (2010) 709–716.
- [12] G. Baffou, R. Quidant, Thermo-plasmonics: using metallic nanostructures as nanosources of heat, Laser Photonics Rev. 7 (2013) 171–187.
- [13] Y. Tian, T. Tatsuma, Mechanisms and applications of plasmon-induced charge separation at TiO₂ films loaded with gold nanoparticles, J. Am. Chem. Soc. 127 (2005) 7632–7637.
- [14] S. Mubeen, G. Hernandez-Sosa, D. Moses, J. Lee, M. Moskovits, Plasmonic photosensitization of a wide band gap semiconductor: converting plasmons to charge carriers, Nano Lett. 11 (2011) 5548–5552.
- [15] D.B. Ingram, S. Linic, Water splitting on composite plasmonic-metal/semiconductor photoelectrodes: evidence for selective plasmon-induced formation of charge carriers near the semiconductor surface, J. Am. Chem. Soc. 133 (14) (2011) 5202–5205.
- [16] C. Gomes Silva, R. Juárez, T. Marino, R. Molinari, H. García, Influence of excitation wavelength (uv or visible light) on the photocatalytic activity of titania containing gold nanoparticles for the generation of hydrogen or oxygen from water, J. Am. Chem. Soc. 133 (3) (2011) 595–602.
- [17] J. Lee, S. Mubeen, X. Ji, G.D. Stucky, M. Moskovits, Plasmonic photoanodes for solar water splitting with visible light, Nano Lett. 12 (9) (2012) 5014–5019.
- [18] I. Thomann, B.A. Pinaud, Z. Chen, B.M. Clemens, T.F. Jaramillo, M.L. Brongersma, Plasmon enhanced solar-to-fuel energy conversion, Nano Lett. 11 (8) (2011) 3440–3446.
- [19] H.M. Chen, C.K. Chen, C.-J. Chen, L.-C. Cheng, P.C. Wu, B.H. Cheng, Y.Z. Ho, M.L. Tseng, Y.-Y. Hsu, T.-S. Chan, J.-F. Lee, R.-S. Liu, D.P. Tsai, Plasmon inducing effects for enhanced photoelectrochemical water splitting: X-ray absorption approach to electronic structures, ACS Nano 6 (8) (2012) 7362–7372.
- [20] S. Mubeen, J. Lee, N. Singh, S. Kramer, G.D. Stucky, M. Moskovits, An autonomous photosynthetic device in which all charge carriers derive from surface plasmons, Nat. Nanotechnol. 8 (2013) 247–251.
- [21] W. Zhang, W. Wang, H. Shi, Y. Liang, J. Fu, M. Zhu, Surface plasmon-driven photoelectrochemical water splitting of aligned ZnO nanorod arrays decorated with loading-controllable Au nanoparticles, Sol. Energy Mater. Sol. Cells 180 (2018) 25–33
- [22] J. Abed, M. AlMheiri, F. Alexander, N.S. Rajput, J. Viegas, M. Jouiad, Enhanced solar absorption of gold plasmon assisted TiO₂-based water splitting composite, Sol. Energy Mater. Sol. Cells 180 (2018) 228–235.
- [23] S. Mukherjee, F. Libisch, N. Large, O. Neumann, L.V. Brown, J. Cheng, J.B. Lassiter, E.A. Carter, P. Nordlander, N.J. Halas, Hot electrons do the impossible: plasmoninduced dissociation of H₂ on Au, Nano Lett. 13 (1) (2013) 240–247.
- [24] S. Mukherjee, L. Zhou, A.M. Goodman, N. Large, C. Ayala-Orozco, Y. Zhang, P. Nordlander, N.J. Halas, Hot-electron-induced dissociation of H₂ on gold nanoparticles supported on SiO₂, J. Am. Chem. Soc. 136 (1) (2014) 64–67.
- [25] P. Christopher, H. Xin, A. Marimuthu, S. Linic, Singular characteristics and unique

- chemical bond activation mechanisms of photocatalytic reactions on plasmonic nanostructures, Nat. Mater. 11 (2012) 1044–1050.
- [26] M. Murdoch, G.I.N. Waterhouse, M.A. Nadeem, J.B. Metson, M.A. Keane, R.F. Howe, J. Llorca, H. Idriss, The effect of gold loading and particle size on photocatalytic hydrogen production from ethanol over Au/TiO₂ nanoparticles, Nat. Chem. 3 (2011) 489–492.
- [27] A. Naldoni, F. Riboni, U. Guler, A. Boltasseva, V.M. Shalaev, A.V. Kildishev, Solar-powered plasmon-enhanced heterogeneous catalysis, Nanophotonics 5 (2016) 112–133.
- [28] L. Guan, X. Chen, Photoexcited charge transport and accumulation in anatase TiO₂, ACS Appl. Energy Mater. 1 (8) (2018) 4313–4320.
- [29] J. Low, B. Cheng, J. Yu, Surface modification and enhanced photocatalytic CO₂ reduction performance of TiO₂: a review, Appl. Surf. Sci. 392 (2017) 658–686.
- [30] D.A. Panayotov, A.I. Frenkel, J.R. Morris, Catalysis and photocatalysis by nanoscale Au/TiO₂: perspectives for renewable energy, ACS Energy Lett. 2 (2017) 1223–1231.
- [31] A. Subrahmanyam, K.P. Biju, P. Rajesh, K.J. Kumar, M.R. Kiran, Surface modification of sol gel TiO₂ surface with sputtered metallic silver for Sun light photocatalytic activity: initial studies, Sol. Energy Mater. Sol. Cells 101 (2012) 241–248.
- [32] S.A. Ansari, M.M. Khan, M.O. Ansari, M.H. Cho, Silver nanoparticles and defect-induced visible light photocatalytic and photoelectrochemical performance of Ag@ m-TiO₂ nanocomposite, Sol. Energy Mater. Sol. Cells 141 (2015) 162–170.
- [33] H. Pan, A. Steiniger, M.D. Heagy, S. Chowdhury, Efficient production of formic acid by simultaneous photoreduction of bicarbonate and oxidation of glycerol on gold-TiO₂ composite under solar light, J. CO2 Util. 22 (2017) 117–123.
- [34] H. Pan, S. Chowdhury, D. Premachandra, S. Olguin, M.D. Heagy, Semiconductor photocatalysis of bicarbonate to solar fuels: formate production from copper(i) oxide, ACS Sustain. Chem. Eng. 6 (2018) 1872–1880.
- [35] S.A. Maier, Plasmonics: Fundamentals and Applications, Springer, New York, 2007.
- [36] G.M. Veith, A.R. Lupini, S. Rashkeev, S.J. Pennycook, D.R. Mullins, V. Schwartz, C.A. Bridges, N.J. Dudney, Thermal stability and catalytic activity of gold nanoparticles supported on silica, J. Catal. 262 (2009) 92–101.
- [37] L. Zhou, C. Zhang, M.J. McClain, A. Manjavacas, C.M. Krauter, S. Tian, F. Berg, H.O. Everitt, E.A. Carter, P. Nordlander, N.J. Halas, Aluminum nanocrystals as a plasmonic photocatalyst for hydrogen dissociation, Nano Lett. 16 (2) (2016) 1478–1484.
- [38] G.V. Naik, J.L. Schroeder, X. Ni, A.V. Kildishev, T.D. Sands, A. Boltasseva, Titanium nitride as a plasmonic material for visible and near-infrared wavelengths, Opt. Mater. Express 2 (2012) 478–489.
- [39] U. Guler, V.M. Shalaev, A. Boltasseva, Nanoparticle plasmonics: going practical with transition metal nitrides. Mater. Today 18 (2015) 227–237.
- [40] P. Patsalas, N. Kalfagiannis, S. Kassavetis, Optical properties and plasmonic performance of titanium nitride. Materials 8 (2015) 3128–3154.
- [41] M. Kumar, S. Ishii, N. Umezawa, T. Nagao, Band engineering of ternary metal nitride system Ti_{1-x} Zr_xN for plasmonic applications, Opt. Mater. Express 6 (2016) 29–38.
- [42] S. Ishii, S.L. Shinde, W. Jevasuwan, N. Fukata, T. Nagao, Hot electron excitation from titanium nitride using visible light, ACS Photonics 3 (2016) 1552–1557.
- [43] A. Lalisse, G. Tessier, J. Plain, G. Baffou, Plasmonic efficiencies of nanoparticles made of metal nitrides (TiN, ZrN) compared with gold, Sci. Rep. 6 (2016) 38647.
- [44] S. Magdi, M.A. Swillam, Investigating several ZrN plasmonic nanostructures and their effect on the absorption of organic solar cells, J. Phys. D 50 (38) (2017) 385501.
- [45] A. Naldoni, U. Guler, Z. Wang, M. Marelli, F. Malara, X. Meng, L.V. Besteiro, A.O. Govorov, A.V. Kildishev, A. Boltasseva, V.M. Shalaev, Broadband hot-electron collection for solar water splitting with plasmonic titanium nitride, Adv. Opt. Mater. 5 (15) (2017) 1601031.
- [46] S. Ishii, S.L. Shinde, T. Nagao, Nonmetallic materials for plasmonic hot carrier excitation, Adv. Opt. Mater 0 (0) (2018) 1800603.
- [47] A. Habib, F. Florio, R. Sundararaman, Hot carrier dynamics in plasmonic transition metal nitrides, J. Opt. 20 (6) (2018) 064001.
- [48] U. Guler, S. Suslov, A.V. Klidishev, A. Boltasseva, V.M. Shalaev, Colloidal plasmonic titanium nitride nanoparticles: properties and applications, Nanophotonics 4 (2015) 269–276.
- [49] S. Ishii, R.P. Sugavaneshwar, K. Chen, T.D. Dao, T. Nagao, Sunlight absorbing titanium nitride nanoparticles, 2015 17th International Conference on Transparent Optical Networks, ICTON, 2015, pp. 1–3.
- [50] O. Anjaneyulu, S. Ishii, T. Imai, T. Tanabe, S. Ueda, T. Nagao, H. Abe, Plasmon-mediated photothermal conversion by TiN nanocubes toward CO oxidation under solar light illumination, RSC Adv. 6 (2016) 110566–110570.
- [51] B.Y. Zheng, H. Zhao, A. Manjavacas, M. McClain, P. Nordlander, N.J. Halas, Distinguishing between plasmon-induced and photoexcited carriers in a device geometry, Nat. Commun. 6 (2015) 7797.
- [52] A. Lalisse, G. Tessier, J. Plain, G. Baffou, Quantifying the efficiency of plasmonic materials for near-field enhancement and photothermal conversion, J. Phys. Chem. C 119 (45) (2015) 25518–25528.
- [53] J.A. Briggs, G.V. Naik, Y. Zhao, T.A. Petach, K. Sahasrabuddhe, D. Goldhaber-Gordon, N.A. Melosh, J.A. Dionne, Temperature-dependent optical properties of titanium nitride, Appl. Phys. Lett. 110 (10) (2017) 101901.

- [54] H. Reddy, U. Guler, Z. Kudyshev, A.V. Kildishev, V.M. Shalaev, A. Boltasseva, Temperature-dependent optical properties of plasmonic titanium nitride thin films, ACS Photonics 4 (2017) 1413–1420.
- [55] M. Kaur, S. Ishii, S.L. Shinde, T. Nagao, All-ceramic solar-driven water purifier based on anodized aluminum oxide and plasmonic titanium nitride, Adv. Sustainable Syst. 3 (2019) 1800112.
- [56] W. Smith, H. Fakhouri, J. Pulpytel, S. Mori, R. Grilli, M.A. Baker, F. Arefi-Khonsari, Visible light water splitting via oxidized tin thin films, J. Phys. Chem. C 116 (2012) 15855–15866
- [57] J. He, J.M. Pringle, Y.-B. Cheng, Titanium carbide and titanium nitride-based nanocomposites as efficient catalysts for the CO2+/CO3+ redox couple in dye-sensitized solar cells, J. Phys. Chem. C 118 (2014) 16818–16824.
- [58] S. Ishii, R.P. Sugavaneshwar, T. Nagao, Titanium nitride nanoparticles as plasmonic solar heat transducers, J. Phys. Chem. C 120 (2016) 2343–2348.
- [59] S.L. Shinde, S. Ishii, T.D. Dao, R.P. Sugavaneshwar, T. Takei, K.K. Nanda, T. Nagao, Enhanced solar light absorption and photoelectrochemical conversion using TiN nanoparticle-incorporated C₃N₄-C dot sheets, ACS Appl. Mater. Interfaces 10 (2018) 2460–2468.
- [60] X. Yu, Z. Zhao, D. Sun, N. Ren, L. Ding, R. Yang, Y. Ji, L. Li, H. Liu, TiO₂/TiN core/shell nanobelts for efficient solar hydrogen generation, Chem. Commun. 54 (2018) 6056–6059.
- [61] A. Álvarez, A. Bansode, A. Urakawa, A.V. Bavykina, T.A. Wezendonk, M. Makkee, J. Gascon, F. Kapteijn, Challenges in the greener production of formates/formic acid, methanol, and DME by heterogeneously catalyzed CO₂ hydrogenation processes, Chem. Rev. 117 (2017) 9804–9838.
- [62] M. Grasemann, G. Laurenczy, Formic acid as a hydrogen source recent developments and future trends, Energy Environ. Sci. 5 (2012) 8171–8181.
- [63] D. Maruthamani, D. Divakar, M. Kumaravel, Enhanced photocatalytic activity of TiO₂ by reduced graphene oxide in mineralization of rhodamine b dye, Ind. Eng. Chem. Res. 30 (2015) 33–43.
- [64] D.P. Leonard, H. Pan, M.D. Heagy, Photocatalyzed reduction of bicarbonate to formate: effect of ZnS crystal structure and positive hole scavenger, ACS Appl. Mater. Interfaces 7 (2015) 24543–24549.
- [65] H. Pan, V.A. Risley, K.R. Martindale, M.D. Heagy, Photocatalytic reduction of bicarbonate to formic acid using hierarchical ZnO nanostructures, ACS Sustain. Chem. Eng. 7 (1) (2019) 1210–1219.
- [66] F.J. García de Abajo, Multiple scattering of radiation in clusters of dielectrics, Phys. Rev. B 60 (1999) 6086–6102.
- [67] T. Siefke, S. Kroker, K. Pfeiffer, O. Puffky, K. Dietrich, D. Franta, I. Ohlídal, A. Szeghalmi, E.-B. Kley, A. Tünnermann, Materials pushing the application limits of wire grid polarizers further into the deep ultraviolet spectral range, Adv. Opt. Mater 4 (2016) 1780–1786.
- [68] P.B. Johnson, R.W. Christy, Optical constants of the noble metals, Phys. Rev. B 6 (1972) 4370–4379.
- [69] ASTM G173-03, Standard Tables for Reference Solar Spectral Irradiances: Direct Normal and Hemispherical on 37° Tilted Surface, ASTM International, West Conshohocken, PA, 2012 2012 https://doi.org/10.1520/G0173-03R12.
- [70] C.J. Stalder, S. Chao, M.S. Wrighton, Electrochemical reduction of aqueous bicarbonate to formate with high current efficiency near the thermodynamic potential at chemically derivatized electrodes, J. Am. Chem. Soc. 106 (1984) 3673–3675.
- [71] M. Bledowski, L. Wang, A. Ramakrishnan, O.V. Khavryuchenko, V.D. Khavryuchenko, P.C. Ricci, J. Strunk, T. Cremer, C. Kolbeckf, R. Beranek, Visible-light photocurrent response of TiO₂-polyheptazine hybrids: evidence for interfacial charge-transfer absorption, Phys. Chem. Chem. Phys. 13 (2011) 21511–21519.
- [72] A. Molinari, L. Samiolo, R. Amadelli, Epr spin trapping evidence of radical intermediates in the photo-reduction of bicarbonate/CO₂ in TiO₂ aqueous suspensions, Photochem. Photobiol. Sci. 14 (2015) 1039–1046.
- [73] C. Di Valentin, D. Fittipaldi, Hole scavenging by organic adsorbates on the TiO₂ surface: a DFT model study, J. Phys. Chem. Lett. 4 (2013) 1901–1906.
- [74] B. Zhou, J. Song, H. Zhou, L. Wu, T. Wu, Z. Liu, B. Han, Light-driven integration of the reduction of nitrobenzene to aniline and the transformation of glycerol into valuable chemicals in water, RSC Adv. 5 (2015) 36347–36352.
- [75] G. Dodekatos, H. Tueysuez, Plasmonic Au/TiO₂ nanostructures for glycerol oxidation, Catal. Sci. Technol. 6 (2016) 7307–7315.
- [76] A.L. González, C. Noguez, Influence of morphology on the optical properties of metal nanoparticles, J. Comput. Theor. Nanosci. 4 (2007) 231–238.
- [77] V. Myroshnychenko, J. Rodríguez-Fernández, I. Pastoriza-Santos, A.M. Funston, C. Novo, P. Mulvaney, L.M. Liz-Marzán, F.J. García de Abajo, Modelling the optical response of gold nanoparticles, Chem. Soc. Rev. 37 (2008) 1792–1805.
- [78] C. Li, W. Yang, L. Liu, W. Sun, Q. Li, In situ growth of TiO₂ on TiN nanoparticles for non-noble-metal plasmonic photocatalysis, RSC Adv. 6 (2016) 72659–72669.
- [79] Infrared spectroscopy absorption table, last updated 2014, https://chem.libretexts. org/Ancillary_Materials/Reference/Reference_Tables /Spectroscopic_Parameters/ Infrared_Spectroscopy_Absorption_Table, (accessed November 2018).
- [80] J.R.S. Brownson, M.I. Tejedor-Tejedor, M.A. Anderson, FTIR spectroscopy of alcohol and formate interactions with mesoporous TiO₂ surfaces, J. Phys. Chem. B 110 (25) (2006) 12494–12499.